Electromechanical characterization of individual micron-sized metal coated polymer particles

Molly Bazilchuk, Sigurd Rolland Pettersen, Helge Kristiansen, Zhiliang Zhang, and Jianying He

Citation: Journal of Applied Physics **119**, 245102 (2016); doi: 10.1063/1.4954218
View online: http://dx.doi.org/10.1063/1.4954218
View Table of Contents: http://scitation.aip.org/content/aip/journal/jap/119/24?ver=pdfcov
Published by the AIP Publishing

JOURNAL OF APPLIED PHYSICS **119**, 245102 (2016)

Electromechanical characterization of individual micron-sized metal coated polymer particles

Molly Bazilchuk,[1,2] Sigurd Rolland Pettersen,[1] Helge Kristiansen,[1,2] Zhiliang Zhang,[1] and Jianying He[1,a)]

[1]*Department of Structural Engineering, Norwegian University of Science and Technology, Trondheim 7491, Norway*

[2]*Conpart AS, Skjetten 2013, Norway*

(Received 15 March 2016; accepted 4 June 2016; published online 22 June 2016)

Micron-sized polymer particles with nanoscale metal coatings are essential in conductive adhesives for electronics assembly. The particles function in a compressed state in the adhesives. The link between mechanical properties and electrical conductivity is thus of the utmost importance in the formation of good electrical contact. A custom flat punch set-up based on nanoindentation has been developed to simultaneously deform and electrically probe individual particles. The set-up has a sufficiently low internal resistance to allow the measurement of sub-Ohm contact resistances. Additionally, the set-up can capture mechanical failure of the particles. Combining this data yields a fundamental understanding of contact behavior. We demonstrate that this method can clearly distinguish between particles of different sizes, with different thicknesses of metal coating, and different metallization schemes. The technique provides good repeatability and physical insight into the behavior of these particles that can guide adhesive design and the optimization of bonding processes. *Published by AIP Publishing.*
[http://dx.doi.org/10.1063/1.4954218]

I. INTRODUCTION

In electronic assembly, conductive adhesives are used in applications that require properties such as low assembly temperature, minimal mechanical stress, and fine pitch.[1] Conductive adhesives compete with lead-free solders as a non-toxic alternative to traditional solder.[2] Micron-sized polymer spheres (MPS) with nanoscale metal coatings are applied as the conductive component in conductive adhesives due to their low cost and superior mechanical characteristics.[1] Conductive adhesives may be either anisotropic or isotropic, and specific applications require different particle sizes, concentrations, and metallization schemes.[2]

In an anisotropic conductive adhesive (ACA), an adhesive film containing conductive particles is compressed between two electrical components. The MPS are deformed under compression, forming contact surfaces against the electrical components. The size and nature of these contact surfaces have a significant effect on the resulting contact resistance. At higher compressive strains, the metal coating, and eventually the particle core, will fracture. Fracture can interrupt the contact and cause increased resistance and decreased long-term performance.[3] The conductive characteristics of the adhesive are therefore strongly linked to the mechanical behavior of MPS under compression, and it is of great interest to find the optimal deformation range where the electrical contact resistance reaches a minimum while still being stable under fatigue.

As a spherical particle is compressed between two rigid plates, the particle expands laterally and the contact area between the particle and the plates increases nonlinearly. Both theoretical and experimental studies of the mechanical properties of individual polymer particles and MPS have been performed. Several models have been proposed to explain the deformation and fracture of particles, incorporating finite element analysis,[4] molecular dynamics simulation,[5] and analytical modeling.[6] Mechanical characterization of individual polymer particles and MPS have been performed by He *et al*. using a custom nanoindentation set-up with a flat punch.[7] The influence of factors such as particle size,[8] polymer cross-linking density,[9] loading rate,[10] and chemical composition on the mechanical behavior has been quantified. Furthermore, the fracture behavior of MPS has been studied.[11] The present work therefore emphasizes the correlation between mechanical behavior and electrical resistance in MPS rather than a detailed analysis of mechanical characteristics.

We shall consider the electrical resistance of the MPS under compression as being the sum of a shell resistance and a contact resistance, as illustrated in Fig. 1. The contact resistance is the resistance experienced by current passing through the area of the particle that is in contact with the object compressing the body. The shell resistance is the resistance due to current passing through the unconstricted areas of metal coating

The contact resistance may be seen as the sum of a constriction term and an interface resistance term. Constriction resistance stems from the geometrical constriction of the current at the interface, essentially a bottleneck of the current. Interface resistance comes from higher resistivity layers that form barriers at the interface, such as oxides.[12] As a rule, contact resistance decreases with increasing contact area.

a)Author to whom correspondence should be addressed. Electronic mail: jianying.he@ntnu.no

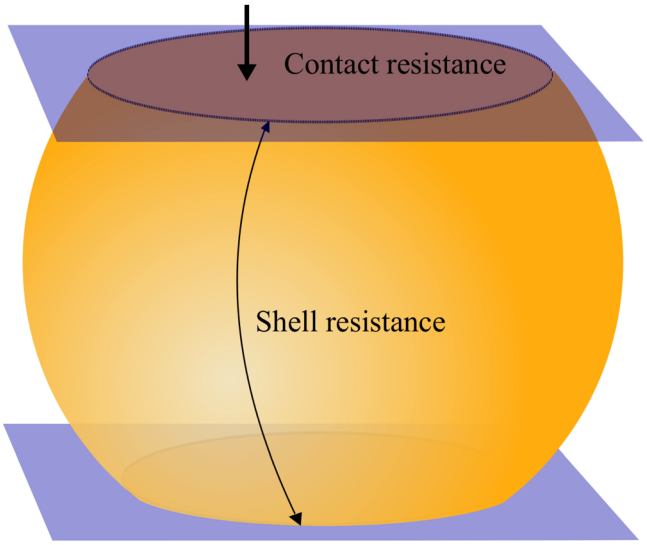

FIG. 1. The resistance of an MPS is the sum of the shell resistance and the contact resistances at either interface.

At the early stages of particle compression, the contact area between the particle and the compressive body is very small, which causes constriction resistance.[13] Furthermore, the true contact area is made up of spots where nanoscale asperities in the contacting bodies meet. Since the true contact is formed in these asperities, the constriction resistance is always larger than the apparent contact area suggests. The shape and distribution of asperities on the surface of the metal coating are unknown, as is their mechanical behavior during the compression of the particle. Additionally, although constriction resistance at semi-infinite (i.e., bulk) metal interfaces has been described analytically,[14] thin metal films will deviate considerably from this theory.[15]

The shell resistance of a single particle depends on the coating thickness t and resistivity ρ, as well as the nominal strain $\varepsilon = \frac{\delta}{D}$, where δ is the deformation and D is the undeformed particle diameter. Määttanen developed an expression for the shell resistance by integrating over the metallic cross-section area of the deformed sphere.[16] The principle assumptions made in this model are that $t \ll D$, where the metal coating is uniform and homogeneous, and the area of the metal coating is constant, i.e., the coating does not crack during compression. It is nonetheless a good first approximation of the shell resistance. Using this model, the expression for the shell resistance is as follows:

$$R_{shell} = \frac{\rho}{\pi t} \ln \tan \frac{\pi}{4}(2 - \varepsilon). \quad (1)$$

Although the current-carrying length through the metal coating increases with particle size, so does the cross-sectional area of the coating. For a given thickness, the increase in resistive length and cross-sectional area cancel each other out and the shell resistance is found to be independent of particle size.

Other attempts to calculate the shell resistance take into account more complex deformation mechanisms, often using a finite element approach.[1] However, none of the previous work has compared the results with the measurements on individual particles, and all predict much lower resistance values than those measured in bulk conductive adhesives.[17] Analyzing the resistance of individual MPS under compression can yield a fundamental understanding that will facilitate the tailoring of particles and the bonding process for electronics assembly.

The body of literature on anisotropic conductive adhesives (ACA) pertaining to electrical resistance focuses on the resistance of bonded ACA joints. This implies many particles in parallel, as in Refs. 17–21. Few attempts have been made to measure the deformation resistance characteristics of single particles. Both Dou *et al.*[22] and Shih *et al.*[23] have reported electromechanical measurements on the ACA particles, but the magnitude of the resistance measurements is such that we may infer a large parasitic resistance skewing the results. Additionally, large particle-to-particle variations lead us to question the accuracy and repeatability of the measurement procedure. In this work, the electromechanical behavior of several MPS is explored by a custom flat punch nanoindentation technique.

II. EXPERIMENTAL

Ten and thirty micron Spherica™ MPS with silver coatings in a variety of thicknesses as well as a gold/nickel bilayer coating were provided by Conpart AS (Skjetten, Norway). The polymer cores are fabricated using the Ugelstad method,[24] and coated using electroless plating. The 10 μm cores (CV = 1.1%, where CV is the coefficient of variation) are made of styrene with a moderate cross-linking density of 20%, and exhibit viscoelastic behavior.[9] The 30 μm cores (CV < 5%) are made of PMMA, with a low cross-linking density of 1%, giving them an elastic-plastic mechanical behavior. Each type of particle will be referred to as follows: 10–100Ag, where the first number is the polymer core diameter in micrometers, the second the coating thickness in nanometers, and the final letters indicate the metallization of the coating. Table I summarizes the particles examined in this work.

During sample preparation, dry particles were suspended in micro-filtered ethanol and dispersed using an ultrasonic bath. Samples consisting of several hundred individual particles of a given type were created by placing a drop of the ethanol-particle solution onto substrates consisting of a silicon wafer sputter-coated with 1 μm of gold and cut into 1.5 × 1.5 cm squares. Two copper wires were glued to the opposing sides of the gold-coated silicon square using isotropic conductive adhesive (ICA). Short-circuit resistance

TABLE I. The different particle types measured in this work.

Particle diameter (μm)	Core chemistry	Coating thickness(es) (nm)	Coating metallization
10	Styrene, cross-linking density 20%	35, 50, 70, 100, 140, 200	Ag
10	Styrene, cross-linking density 20%	120 Ni + 30 Au	Ni/Au
30	PMMA, cross-linking density 1%	60, 100, 150, 270	Ag

measurements between the copper wires confirmed good contact between the gold film and ICA.

The Hysitron Triboindenter 950 (Minneapolis, USA) is a commercially available nanoindentation system that operates in load-controlled mode with a force resolution <2 nN. The nanoscale electrical contact resistance tool, abbreviated nanoECR, is an additional module that allows precise, correlated electrical and mechanical indentation measurements. Current or voltage can be sourced and measured across a conductive nanoindentation tip, sample, and conductive stage during selected segments of the indentation cycle. The nanoECR module has been previously used in a high-resolution application to investigate an electrical current spike associated with nanoscale plasticity in gallium arsenide.[25]

The commercial nanoECR set-up was designed to measure relatively high resistances in semiconductor samples, and has been modified to facilitate the measurement of sub-Ohm resistances occurring in individual MPS. The aforementioned custom conductive substrates were connected directly to the current and voltage leads in the Triboindenter, bypassing the nanoECR stage. Fig. 2 shows a schematic of the electromechanical measurements performed.

In the work of He *et al.*,[6–10] a diamond flat punch was used to indent single particles. In this work, the indenter was required to be highly conductive in addition to hard, and thus a tungsten carbide flat punch with a diameter of 50 μm fabricated by Synton-MDP (Nidau, Switzerland) was employed.

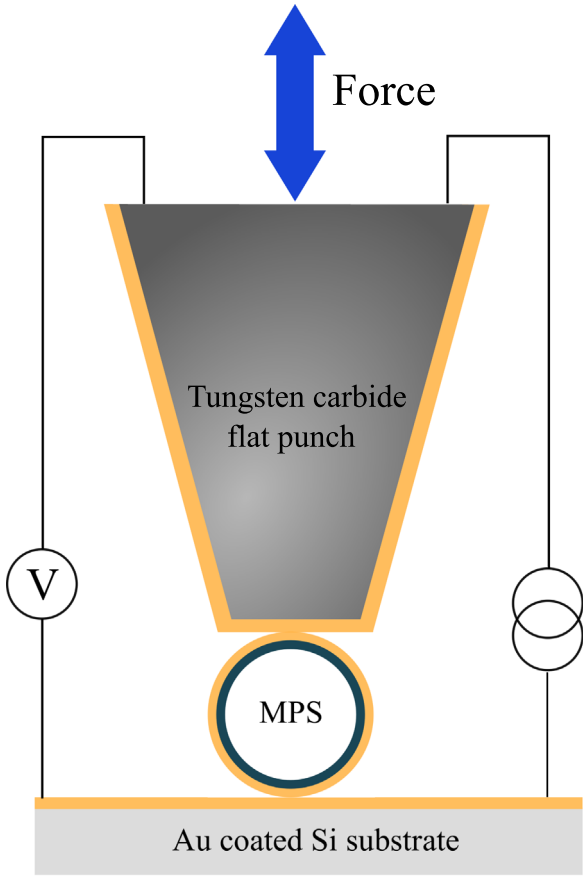

FIG. 2. A schematic showing the principle of the electromechanical measurements conducted in this study.

The tip was dry etched in argon plasma and subsequently sputter-coated with 150 nm of gold in order to maintain a highly conductive surface. Before performing measurements, tip planarity was verified by indenting on a planar indium sample, and low resistance confirmed by performing test indents directly on the gold-coated silicon substrate.

Isolated single particles, at least 50 μm from any neighboring particles, were identified using the optical microscope in the Triboindenter. To remove the influence of the lead resistance, measurements were conducted in 4-wire mode, with the wires connected as shown in Fig. 2. Resistance was obtained by dividing the measured voltage by the sourced current value. To test for Ohmic behavior, measurements including current sweeps were performed on several occasions. These measurements confirmed the linearity of the resistance characteristics within the relevant, albeit small, voltage range.

Due to the placement of the current and voltage wires on the substrate as shown in Fig. 2, the measurement encompassed the indentation tip, the MPS, and part of the substrate. The measured resistance was thus comprised of a series of resistances,

$$R_{measured} = R_{tip} + R_{contact\,tip-MPS} + R_{shell} + R_{contact\,MPS-substrate} + R_{substrate}. \quad (2)$$

The true resistance of the MPS, or the shell and contact resistances, will be always smaller than the measured resistance, although the highly conductive probe and substrate reduce parasitic resistances. The resistance contributions from the probe R_{tip} and substrate $R_{substrate}$ have been considered to be independent of particle deformation, although in reality there is a contact resistance at their interfaces for which this is not entirely the case.

All electrical measurements were conducted with a sourced current of 1 mA, selected because it was large enough to give a good signal but small enough to avoid sufficient heating to alter the mechanical behavior of the particles. The current was switched on 0.2 s after the initial contact was achieved, as shown in Fig. 3, in order to ensure sufficient thermal contact before the electrical measurement was initiated. The mechanical indentation data of several types of particles with and without applied current were compared, and it was confirmed that any Joule heating did not visibly alter the mechanical results.

In all measurements, force was applied at a constant rate of 2 mN/s, up to a maximum of 12 mN, as shown in Fig. 3. This maximum force value was limited by the Triboindenter equipment. The maximum force was then held for 2 s before being released at the same rate. The resulting mechanical deformation of the particles was monitored continuously throughout the loading cycle.

III. RESULTS AND DISCUSSION

A. Representative electromechanical behavior

Fig. 4 shows the result of a typical electromechanical measurement for a 10–100Ag particle. The measured

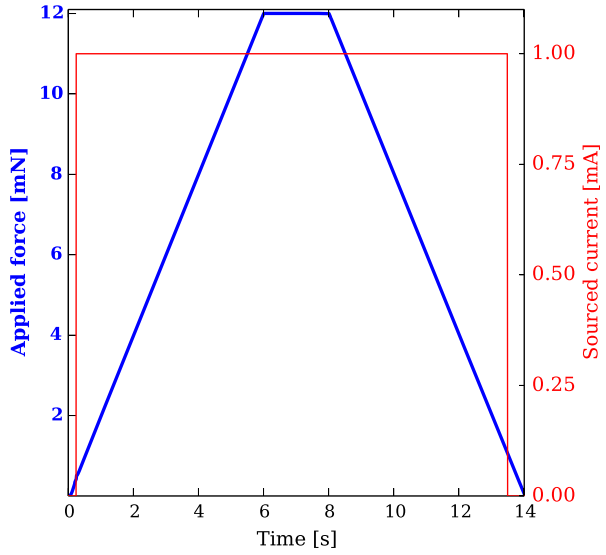

FIG. 3. The representative load and current function for the electromechanical measurements performed on MPS.

resistance depends strongly on the applied force, indicating that the resistance of the MPS is significant in the measurement. Excluding Fig. 4, all the results presented in this work reflect statistical averages of 8–10 particles where the error bars represent the standard deviation. This contributes to verifying the uniformity and repeatability of the results.

In Fig. 4, the measured resistance can be seen to decrease rapidly during the initial stages of loading, and level off for large applied forces. As the particle is compressed, the contact area at the particle interfaces increases while the current-carrying length through the coating decreases. The decrease in resistance can be attributed to a combination of these changes.

At the rate the particle is unloaded, the core does not have sufficient time for viscoelastic recovery, so the measurement ends at a high strain of 40%. However, the measured resistance increases gradually during unloading. This indicates an elastic rebound, causing the tip to remain in contact during unloading, rather than an abrupt loss of contact as would be expected if the particle were permanently deformed.

B. Effect of particle size

Fig. 5 shows a comparison of the resistance-strain behavior of 30–100Ag and 10–100Ag. The MPS differ both in size and core material, but the coatings are the same thickness and material. The measurements for 30–100Ag stop at a much lower strain than 10–100Ag because the same force produces a lower strain in the larger particles, and the largest available force is only enough to produce around 5% strain.

The Määttanen model for the shell resistance as described by Eq. (1) predicts that the resistance of metal coating is independent of the particle size, depending only on the strain, coating thickness, and resistivity. We therefore consider the R_{shell} contribution in Eq. (2) to be equal for 30–100Ag and 10–100Ag at a given strain. The discrepancies between the two curves can therefore be attributed to

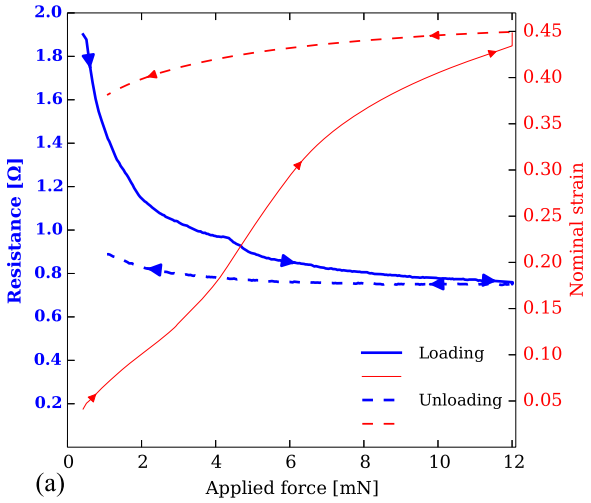

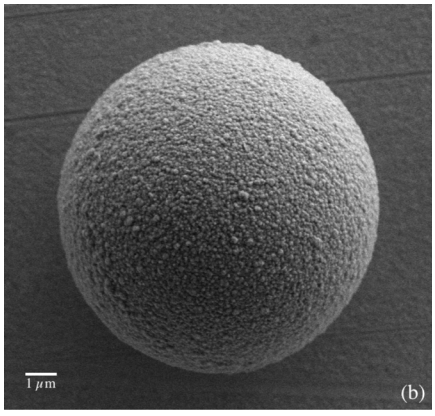

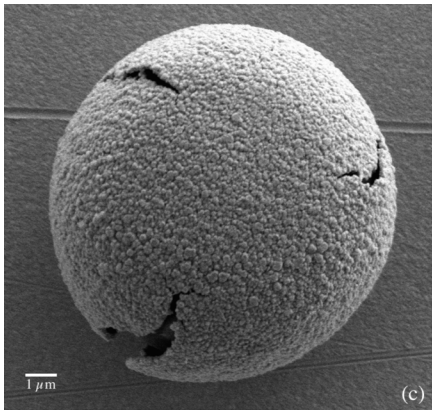

FIG. 4. Representative electromechanical results for particle type 10-100Ag (a), where the deformation and resistance have been monitored as a function of the applied force. Arrows denote the direction of the measurement in time. Micrographs showing a particle before (b) and after (c) compression.

the contact resistance contributions in Eq. (2), $R_{contact\ tip-MPS}$ and $R_{contact\ MPS-substrate}$ both of which depend on the contact area. Since the contact area increases radially and thus scales with the square of the particle size, it increases more rapidly in 30–100Ag, yielding the lower resistances observed at small strains.

The standard deviation of the resistance at a given strain is indicated by the error bars in Fig. 4, and represents the particle-to-particle variability of the measurement. Uniform resistance characteristics in MPS are desirable because they

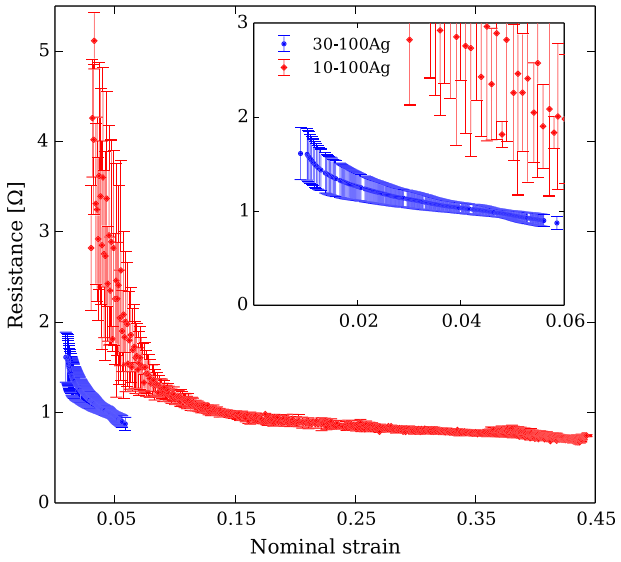

FIG. 5. The resistance-strain characteristics of 30-100Ag and 10-100Ag. The inset is a close-up of the 30-100 Ag curve.

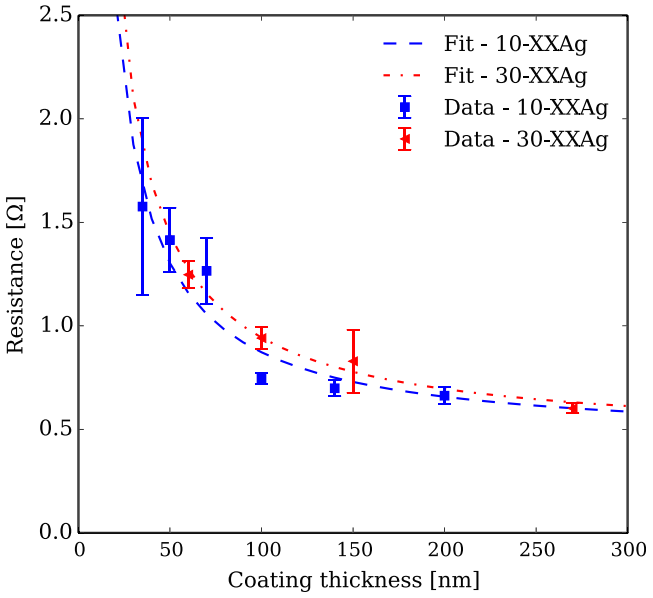

FIG. 6. The average resistance at 10 mN applied force for 10 and 30 μm particles with different coating thicknesses. The resistances are taken at 40% and 5% strain, respectively. The curves have been fit to Eq. (3).

give an adhesive with predictable behavior. The low particle-to-particle variability at high strain confirms the stability and repeatability of the measurements. At 40% strain, the particle-to-particle variability of 10–100Ag is 6%. By comparison, particle-to-particle variability measured by Dou *et al.* was 35% at 40% strain.[22]

As indicated by the error bars in Fig. 5, the particle-to-particle variability in the resistance is largest during the initial stages of deformation. This can be attributed to the nanoscopic asperities in the coating, the distribution of which varies from particle to particle. At higher strains, the behavior becomes more uniform. At this point, the contact area has grown large enough for the contact resistance to have a negligible contribution to the measured resistance. The measured resistance is then governed by coating resistivity and thickness, which are relatively uniform for particles from the same batch.

C. Effect of coating thickness

The effect of coating thickness on the resistance characteristics has been analyzed for the 10-XXAg and 30-XXAg series by comparing the particles at the highest available applied strain, in order to minimize the contribution of contact resistance, which is largest at low strains. Ten micron particles with different coating thicknesses have been compared at 40% strain and 30 μm particles at 5% strain, again limited by the maximum available force.

As shown in Eq. (1), the coating thickness is expected to be inversely proportional to the shell resistance. To evaluate the effect of the coating thickness, R_{tip}, $R_{contact\,tip-MPS}$, $R_{contact\,MPS-substrate}$, and $R_{substrate}$ are all assumed to be independent of thickness and constant for a given strain. These contributions are lumped into a constant resistance R_{cst}. According to Eq. (2), the remaining resistance contribution is the shell resistance. The measured resistance may be expressed by the following equation:

$$R = \frac{c}{t} + R_{cst}, \tag{3}$$

where t is the coating thickness and c is the fitting constant. Fig. 6 shows 10-AgXX and 30-AgXX fit to Eq. (3).

In order to equate the fit parameter to a meaningful value, we will assume that the shell resistance follows Eq. (1). The strain ε is well-known due to the high resolution of the nanoindenter system. The conductivity ρ, however, may deviate from the bulk value $\rho_{Ag} = 1.59 \times 10^{-8}\,\Omega\,\mathrm{m}$[26] and the coating thickness t is a nominal, not measured, value. We thus multiply Eq. (1) with an ideality factor m which describes how the ratio between ρ and t deviates from the ideal case. By equating Eq. (1) to the thickness-dependent term in Eq. (3) and rearranging, we find an expression for the ideality factor

$$m = \frac{c\,\pi}{\rho_{Ag} \ln \tan \frac{\pi}{4}(2-\varepsilon)}. \tag{4}$$

Table II summarizes the fitting parameters and calculates the ideality factors for each case.

The ideality factor m is larger than unity for both sets of particles. This could indicate either that the coatings are thinner than their nominal value or that the resistivity is higher than that of bulk silver. The resistivity of thin metal films is known to deviate from the bulk resistivity values.[27] This effect is significant when the film thickness or grain size approaches the electron mean free path (EMFP), which is 52 nm for bulk silver.[26] However, surface and grain boundary scattering limited resistivity can only account for a

TABLE II. The fitting parameters used to fit Eq. (3) to the curves in Fig. 6, and the ideality factor m as expressed by Eq. (4).

Particle group	R_{cst} (Ω)	c (Ω nm)	m
10-XXAg	0.44	43.0	7.6
30-XXAg	0.45	49.6	3.0

twofold increase of the resistivity at room temperature.[26] Therefore, other non-idealities must also be considered.

Larger than ideal resistivity could also stem from impurities in the coating due to chemicals used in the coating process or coating roughness which would cause "bottlenecks" in the current flow. It is likely that the non-ideal behavior of the coatings is due to a combination of impurities in the coating, unevenness and surface and grain boundary scattering limited resistivity. The decoupling of these contributions requires further investigation.

Figs. 7(a) and 7(b) show the effect of the coating thickness on the particle-to-particle variability of the resistance characteristics, which can be observed to decrease with increasing coating thickness. The thinner the coating, the more impact uneven areas in the coating will have on the shell resistance, through the creation of bottlenecks in thin areas of the coating. The most uniform behavior is consistently observed in the thickest metal coatings. The variability is largest during the early stages of the deformation (most clearly illustrated by 10–35Ag in Fig. 7), as has previously been discussed for Fig. 4.

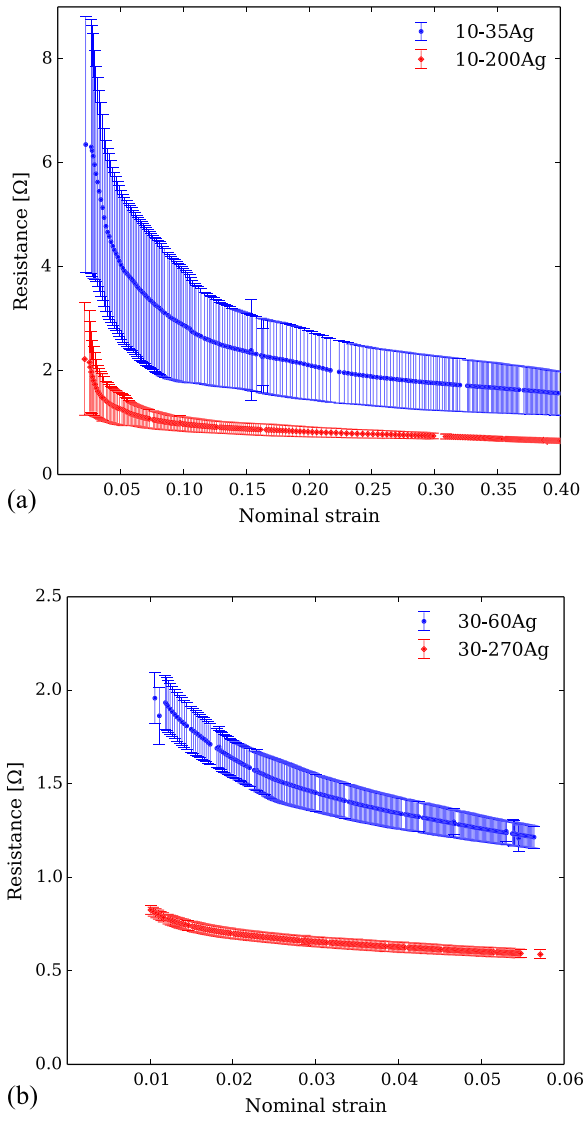

FIG. 7. A comparison of the average resistance-strain characteristics of (a) 10-35Ag and 10-200Ag; and (b) 30-60Ag and 30-270Ag, where the error bars represent the particle to particle variability.

D. Effect of metallization

The effect of the metallization scheme was compared using 10–140Ag and 10–120Ni/30Au, which have the same polymer core and comparable metal coating thicknesses. Figure 8 shows the mechanical behavior, while Fig. 9 compares the resistance-strain characteristics. The nominal stress is given by $\sigma = \frac{F}{\pi(0.5\times D)^2}$, where F is the applied force, while the nominal strain, as previously mentioned, is found by $\varepsilon = \frac{\delta}{D}$.

Mechanically, the nickel-gold system is more brittle than the silver system. In Fig. 8, we can clearly see that 10–120Ni/30Au is stiffer than 10–140Ag initially, due to the mechanical stiffness of nickel. At a strain of approximately 0.2, a pop-in or displacement burst occurs. Since the measurement is load controlled, a sudden movement of the sample causes a displacement burst and an apparent gap in the data. Pop-ins have previously been demonstrated to be indicative of brittle fracture of the metal coating.[10] The particle-to-particle variability is largest in the pop-in region, due to variations in exactly when the pop-in occurs. After the pop-in, the stiffness of the system is decreased, since the coating has been significantly weakened by cracking. In contrast, 10–140Ag exhibits a continuous stress-strain behavior with no pop-ins. The silver coating is ductile, and fractures gradually rather than abruptly. Although the coating is a relatively small part of the particle, it clearly contributes significantly to the mechanical strength of the particles.

Fig. 9 shows the effect of the metallization on the electromechanical behavior. Initially, the high particle-to-particle variability renders the particles virtually indistinguishable. At high strains, the resistance of 10–140Ag converges to a significantly lower value than 10–120Ni/30Au. This follows the expectation based on bulk silver, where the resistivity is lower

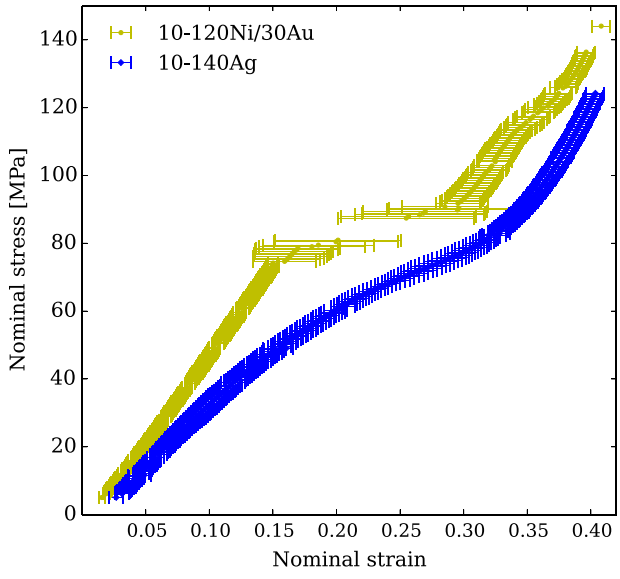

FIG. 8. A comparison of the stress-strain characteristics of 10-140Ag and 10-120Ni/30Au.

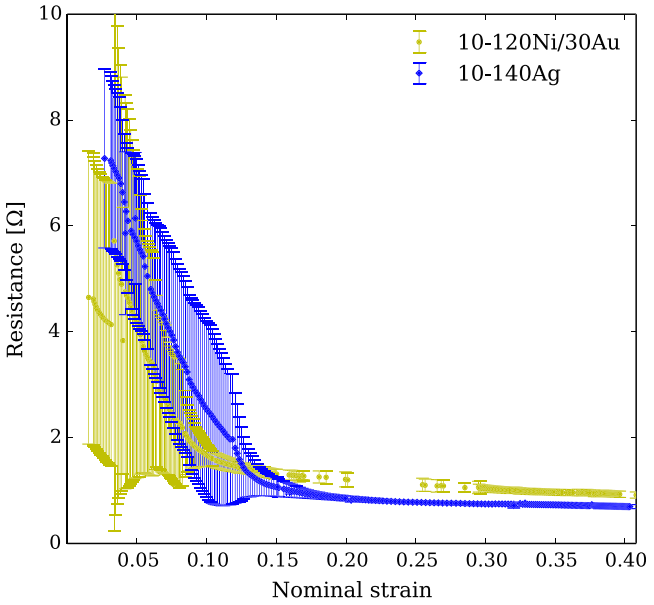

FIG. 9. A comparison of the average resistance-strain characteristics of 10-140Ag and 10-120Ni/30Au.

than that of both bulk nickel and gold. These measurements demonstrate that the set-up is sensitive enough to distinguish between coatings of different materials but similar thicknesses.

Again, a pop-in can be observed in the 10–120Ni/30Au curve, indicating brittle fracture of the metal coating. The gradient of the resistance-strain curve is not visibly affected by the pop-in, suggesting that cracking occurs parallel to the direction of applied force rather than circumferentially. Longitudinal fracture has previously been observed in the Ni/Au system,[11] and a similar fracture pattern is confirmed by SEM images of the Ag system after compression, as shown in Fig. 4(c).

IV. CONCLUSION

Our flat-punch electromechanical nanoindentation technique has been used to measure individual MPS. The measurements are repeatable and precise, and can be used to clearly distinguish different MPS. By studying resistance as a function of strain, we can easily locate the range where the contact resistance has converged to a semi-constant, negligible value, which is useful in the context of the conductive adhesive application. For 10 μm particles, it is observed that the gains in resistance are minimal once the strain passes 15%. Thirty micron particles achieve low resistance values at an earlier stage of deformation.

The measured resistance displays an inverse proportional relationship to the particle coating thickness as expected. The decrease in resistance is therefore most significant when increasing thicknesses up to 100 nm, after which the gains are much smaller. The effect of the metallization scheme on the resistance follows the trends in bulk resistivity of the metallization scheme. However, the mechanical behavior is affected significantly by the metallization of the coating. Both the mechanical behavior and the particle resistance can thus be tuned by changing the metallization and coating thickness.

The measured resistance is a sum of several contributions which cannot be decoupled using this method alone; however, it gives good indications of the relative conductivity of different MPS, and an upper limit of the resistance of single MPS, which has not previously been measured at this level of detail.

ACKNOWLEDGMENTS

The Research Council of Norway provided funding through Projects No. 228453—"Novel Particle Technology for Display Interconnect" and 225962—"Novel Conductive Adhesive Technology for Solar Industry." Partial funding has also been obtained from the Programme FP7-NMP-2013-LARGE-7 under Grant Agreement No. 604668 ("Quantiheat") and by funding from the European Union Seventh Framework Programme (FP7/2007-2013) under Grant Agreement No. FP7-NMP- 310420 ("HyperConnect").

[1]Y. C. Lin and J. Zhong, "A review of the influencing factors on anisotropic conductive adhesives joining technology in electrical applications," J. Mater. Sci. **43**(9), 3072–3093 (2008).
[2]Y. Li and C. P. Wong, "Recent advances of conductive adhesives as a lead-free alternative in electronic packaging: Materials, processing, reliability and applications," Mater. Sci. Eng. R **51**(1–3), 1–35 (2006).
[3]Y. Chan and D. Luk, "Effects of bonding parameters on the reliability performance of anisotropic conductive adhesive interconnects for flip-chip-on-flex packages assembly II. Different bonding pressure," Microelectron. Reliab. **42**(8), 1195–1204 (2002).
[4]Z. L. Zhang, H. Kristiansen, and J. Liu, "A method for determining elastic properties of micron-sized polymer particles by using flat punch test," Comput. Mater. Sci. **39**(2), 305–314 (2007).
[5]J. Wu, S. Nagao, Z. Zhang, and J. He, "Deformation and fracture of nano-sized metal-coated polymer particles: A molecular dynamics study," Eng. Fract. Mech. **150**, 209–221 (2015).
[6]J. Paul, S. Romeis, J. Tomas, and W. Peukert, "A review of models for single particle compression and their application to silica microspheres," Adv. Powder Technol. **25**(1), 136–153 (2014).
[7]J. Y. He, Z. L. Zhang, and H. Kristiansen, "Nanomechanical characterization of single micron-size polymer particles," J. Appl. Polym. Sci. **113**(3), 1398–1405 (2009).
[8]J. Y. He, Z. L. Zhang, M. Midttun, G. Fonnum, G. I. Modahl, H. Kristiansen, and K. Redford, "Size effect on mechanical properties of micron-sized PS–DVB polymer particles," Polymer **49**(18), 3993–3999 (2008).
[9]J. Y. He, Z. L. Zhang, H. Kristiansen, K. Redford, G. Fonnum, and G. I. Modahl, "Crosslinking effect on the deformation and fracture of monodisperse polystyrene-co-divinylbenzene particles," Express Polym. Lett. **7**(4), 365–374 (2013).
[10]J. Y. He, S. Nagao, H. Kristiansen, and Z. L. Zhang, "Loading rate effects on the fracture of Ni/Au nano-coated acrylic particles," Express Polym. Lett. **6**(3), 198–203 (2012).
[11]J. Y. He, T. Helland, Z. L. Zhang, and H. Kristiansen, "Fracture of micrometre-sized Ni/Au coated polymer particles," J. Phys. D: Appl. Phys. **42**(8), 085405 (2009).
[12]R. S. Timsit, "Electrical contact resistance: Fundamental principles," in *Electrical Contacts: Principles and Applications*, edited by P. G. Slade (CRC Press, 2014), pp. 3–111.
[13]J. H. Constable, "Analysis of ACF contact resistance," in *IPACK03*, 2003, pp. 1–8.
[14]J. A. Greenwood, "Constriction resistance and the real area of contact," Br. J. Appl. Phys. **17**(12), 1621–1632 (1966).
[15]R. S. Timsit, "Constriction resistance of thin film contacts," IEEE Trans. Compon. Packag. Technol. **33**(3), 636–642 (2010).
[16]J. Määttänen, "Contact resistance of metal-coated polymer particles used in anisotropically conductive adhesives," Soldering Surf. MountTechnol. **15**(1), 12–15 (2003).

[17]M. Chin, K. A. Iyer, and S. J. Hu, "Prediction of electrical contact resistance for anisotropic conductive adhesive assemblies," IEEE Trans. Compon. Packag. Technol. **27**(2), 317–326 (2004).
[18]M. J. Yim and K. W. Paik, "The contact resistance and reliability of anisotropically conductive film (ACF)," IEEE Trans. Adv. Packag. **22**(2), 166–173 (1999).
[19]M. A. Uddin, M. O. Alam, Y. C. Chan, and H. P. Chan, "Adhesion strength and contact resistance of flip chip on flex packages—effect of curing degree of anisotropic conductive film," Microelectron. Reliab. **44**(3), 505–514 (2004).
[20]C. K. Chung and K. W. Paik, "Effects of the degree of cure on the electrical and mechanical behavior of anisotropic conductive films," J. Electron. Mater. **39**(4), 410–418 (2010).
[21]C. K. Chung, G. D. Sim, S. B. Lee, and K. W. Paik, "Effects of conductive particles on the electrical stability and reliability of anisotropic conductive film chip-on-board interconnections," IEEE Trans. Compon., Packag., Manuf. Technol. **2**(3), 359–366 (2012).
[22]G. Dou, D. Whalley, and C. Liu, "Mechanical and electrical characterisation of individual ACA conductor particles," in *2006 International Conference on Electronic Materials and Packaging* (2006), pp. 1–9.
[23]C. Shih, K. Chen, and H. Li, "Mechanical and electrical properties investigation of micro-size single metal-coated polymer particle," in *ICEP-IAAC 2015 Proceedings* (2015), pp. 527–531.
[24]J. Ugelstad, A. Berge, T. Ellingsen, R. Schmid, T.-N. Nilsen, P. C. Mørk, P. Stenstad, E. Hornes, and Ø. Olsvik, "Preparation and application of new monosized polymer particles," Prog. Polym. Sci. **17**(1), 87–161 (1992).
[25]R. Nowak, D. Chrobak, S. Nagao, D. Vodnick, M. Berg, A. Tukiainen, and M. Pessa, "An electric current spike linked to nanoscale plasticity," Nat. Nanotechnol. **4**(5), 287–291 (2009).
[26]W. Zhang, S. H. Brongersma, O. Richard, B. Brijs, R. Palmans, L. Froyen, and K. Maex, "Influence of the electron mean free path on the resistivity of thin metal films," Microelectron. Eng. **76**(1–4), 146–152 (2004).
[27]D. C. Larson and B. T. Boiko, "Electrical resistivity of thin epitaxially grown silver films," Appl. Phys. Lett. **5**(8), 155–156 (1964).